

Article

# Design and Application of Laser Polarization Underwater Detection Equipment

Yong Zhu <sup>1</sup>, Fangxing Zong <sup>2</sup>, Chao Dong <sup>2</sup>, Qiang Fu <sup>2,3,\*</sup>, Xiansong Gu <sup>2</sup>, Qingyi He <sup>2</sup>, Jianhua Liu <sup>3</sup>, Li Zheng <sup>3</sup>, Geng Dong <sup>3</sup>, Haili Zhao <sup>4</sup> and Jin Duan <sup>4</sup>

<sup>1</sup> College of Computer Science and Technology, Changchun University of Science and Technology, Changchun 130022, China

<sup>2</sup> National and Local Joint Engineering Research Center of Space Optoelectronics Technology, Changchun University of Science and Technology, Changchun 130022, China

<sup>3</sup> College of Opto-Electronic Engineering, Changchun University of Science and Technology, Changchun 130022, China

<sup>4</sup> College of Electronic Information Engineering, Changchun University of Science and Technology, Changchun 130022, China

\* Correspondence: cust\_fuqiang@163.com

**Abstract:** With the increasing demand for precise identification of underwater targets, the development of advanced underwater detection technologies has become a pivotal area of research. This study presents the design and implementation of a laser-based underwater detection system that leverages polarization characteristics to significantly enhance detection accuracy and target identification capabilities in complex aquatic environments. A key innovation of this research lies in the application of a dual-frequency modulation technology using a 532 nm pulsed laser. By modulating the high-frequency characteristics of the laser, this technique effectively suppresses backscattering interference within the water medium, improves the efficiency of target signal extraction, and exhibits exceptional performance, particularly in long-range detection and highly turbid water conditions. This paper elucidates the principles of underwater laser detection and polarization measurement, outlines the design of an integrated optical and mechanical system for laser transmission and reception, and introduces an optimized signal processing methodology. Experimental results demonstrate that the proposed system can reliably distinguish targets composed of different materials while maintaining high detection accuracy across a range of challenging environmental conditions. A comparative analysis further highlights the system's significant advantages over traditional technologies, including enhanced noise suppression and greater detection depth. These findings establish a solid foundation for advancing underwater detection technologies and broadening their practical applications.

**Keywords:** polarization measurements; laser polarization underwater detection; optical system design; dual-frequency modulation; split amplitude; target material



Received: 16 October 2024  
Revised: 27 November 2024  
Accepted: 6 December 2024  
Published: 28 January 2025

**Citation:** Zhu, Y.; Zong, F.; Dong, C.; Fu, Q.; Gu, X.; He, Q.; Liu, J.; Zheng, L.; Dong, G.; Zhao, H.; et al. Design and Application of Laser Polarization Underwater Detection Equipment. *Photonics* **2025**, *12*, 118. <https://doi.org/10.3390/photonics12020118>

**Copyright:** © 2025 by the authors. Licensee MDPI, Basel, Switzerland. This article is an open access article distributed under the terms and conditions of the Creative Commons Attribution (CC BY) license (<https://creativecommons.org/licenses/by/4.0/>).

## 1. Introduction

The ocean is a particularly important part of the ecosystem upon which mankind depends for survival. The vast sea areas are rich in resources such as marine power, marine organisms, seabed minerals, and seawater chemistry, the development and protection of which have gradually received extensive attention from various countries and peoples [1]. Therefore, the development and advancement of underwater target detection and identification technologies hold broad application potential and significant civil and military

value [2]. However, the complexity of the underwater environment presents significant challenges to LIDAR-based underwater detection, particularly due to the absorption and scattering of light by water and suspended particles, which greatly reduce detection range and imaging contrast [3,4].

In the late 1960s, Hickman and Hogg of Syracuse University in the United States manufactured the first laser seawater detection system, which they used to verify the feasibility of laser bathymetry, and initially established the theoretical and experimental basis of underwater laser detection technology [5]. In 1990, Jack Cariou and Bernad Le Jenue from France carried out the first research work on polarization detection of underwater targets [6]. In their research, they chose a 532 nm laser as the light source and a photomultiplier tube as the detector, carried out experiments on the depolarization of seawater and artificial targets in seawater, and calculated the Muller matrix related to the depolarization through the experimental results. Mullenl et al. first proposed a new HybridLidar-radar (HLR) technology combining microwave radar and Lidar in 1995 [7]. The HLR technology uses an optical carrier with high-frequency intensity modulation to filter out the backward scattering, which improves the performance of the system, because the modulation of backward scattering starts to be de-correlated in the high-frequency band (>100 MHz) when the modulation frequency is above 100 MHz, i.e., backscattering loses modulation information in the high-frequency band (>100 MHz) [8]. In 2001, Alexander P. Vasilkov and Yury A. Goldin et al. used airborne lidar to detect the seawater scattering layer and measured the depth of the sea floor along with the seawater scattering coefficients of the vertically layered structure [9]. In 2004, M. Preda used a pulsed laser as a light source and a CCD as a photodetector to irradiate dust plasma, which proved to be a depolarized medium, and in addition to absorption, it would also scatter the incident light and the intensity distribution of the incident light would be changed. In addition, due to the instability of the polarization state of the incident light, the degree of depolarization cannot be detected precisely, but the average degree of depolarization of the polarized image can be easily obtained by a specific polarization detection system [10,11]. In 2010, Yao Tianfu et al. set up a simple experimental system of detecting underwater targets and detected man-made targets made of different materials. The results show that targets of different materials have different polarization characteristics, and the polarization information is of great value for improving the performance of underwater artificial detection [12]. In 2012, Opte turbid company of Canada successfully developed CZM positive airborne laser bathymetry system, which is a new generation of bathymetry and coastal topography detection system with high spatial resolution, large optical aperture, and suitable for poorer water bodies [13]. In 2018, Mou Chang et al. detected underwater targets by establishing an underwater target detection system based on polarization information. They utilized a 532 nm wavelength laser as an active laser transmitter and combined laser underwater detection technology and polarization detection technology. By analyzing the polarization characteristics of the reflected light, results were obtained that underwater targets with different materials and surface structures (e.g., iron, plastic, and water plants) have different polarization degrees. The experiments show that the polarization of reflected light from man-made targets is significantly higher than that of natural targets, thus demonstrating the feasibility of underwater target detection technology based on polarization information.

Building on the foundation of previous studies, while the feasibility of laser and polarization technologies for underwater target detection has been preliminarily demonstrated, challenges such as the effective suppression of backscattering interference, limited detection depth, and constrained target recognition accuracy persist. This study proposes an innovative approach that addresses these limitations by introducing a dual-frequency modulated 532 nm pulsed laser, which effectively mitigates backscattering interference

in detection signals and significantly enhances the efficiency of signal extraction and detection depth [14].

Furthermore, by combining the split-amplitude method with a high-sensitivity optical detection system, the Stokes parameters and polarization characteristics of the target are systematically measured, enabling precise differentiation of targets composed of different materials. In comparison with earlier studies that utilized single-frequency lasers or conventional polarization detection techniques, this research optimizes the optical-mechanical system for laser transmission and reception. It incorporates a narrow-band filter and polarization-splitting prism, which collectively reduce background noise, enhance the device's anti-interference capabilities, and improve signal extraction performance [15].

Extensive experiments conducted in a laboratory-simulated underwater environment demonstrate that the proposed device exhibits significant advantages in terms of detection range, depth, and adaptability to complex conditions. These findings provide valuable insights and a solid reference for advancing underwater detection technologies.

## 2. Detection Principles

### 2.1. Laser Backscattering Frequency Characteristics

The laser power of a laser transmitted in water and returned to a point by encountering a target in water can be viewed in the time domain as the convolution of the incident laser with the impulse response of the water, which can be expressed as [16] follows:

$$P_{dL}(t) = P(t) \otimes H_{dL}(t) \tag{1}$$

where  $P_{dL}(t)$  is the signal of the return laser pulse received at a point  $P_d$ ;  $L$  is the distance from the point  $P_d$  to the target;  $P(t)$  is the laser emission power;  $H_{dL}(t)$  is the impulse response of the water;  $\otimes$  is the convolution operation. The impulse response of the water consists of two parts: the backscattering part  $H_i$  and the target signal part  $H_t$ .

$$H_{dL}(t) = H_i(t) \otimes H_t(t) \tag{2}$$

Equation (2) is Fourier transformed and the frequency response of water can be expressed as follows:

$$H_{dL}(f) = H_i(f) + H_t(f) = \left( \frac{\eta F A_r}{R^2} \right) \cdot \left[ \rho \frac{1 - e^{-2\alpha v t_d} e^{j4\pi f t_d}}{\alpha v - j2\pi f} + \rho_t e^{-2\alpha v t_i} e^{j4\pi f t_i} \right] \tag{3}$$

where  $H_i(f)$  is the frequency-domain component of the continuous backscattering component from the water column;  $H_t(f)$  is the frequency-domain component from the target component;  $\eta$  is the total optical efficiency of the transmitting and receiving systems;  $F$  is the finite field of view;  $A_r$  is the effective receiving aperture area;  $R$  is the detection distance;  $\rho$  is the scattering rate of the seawater (seawater is considered to be a homogeneous medium);  $\alpha$  is the attenuation coefficient of the seawater;  $\rho_t$  is the reflectivity of the target;  $v$  is the rate of light in the seawater;  $t_d$  is the time for the photon to reach the underwater target;  $t_i$  is the one-way return time [17].

According to Equation (3) and the parameters in Table 1, the amplitude-frequency curves of backward scattering and target can be obtained as shown in Figure 1. It can be seen that the amplitude-frequency response of the target signal at different frequencies is unchanged; while the backscattered amplitude-frequency response increases with frequency, the amplitude of the exponential decay, which indicates that the energy of backscattering is mainly concentrated in the low-frequency region [18]. If the laser is emitted after high-frequency intensity modulation, the target signal still has high-frequency character-

istics after transmission in seawater and returns to the target, while the high-frequency component of the backward-scattered signal is lost in the transmission process, and most of the energy is concentrated in the low-frequency component. Therefore, the laser by high-frequency intensity modulation returns to the target signal and backward scattering signal energy in an order of magnitude, the use of high-pass or band-pass filtering can be achieved to inhibit the effect of seawater backward scattering. If the backscattered energy is much smaller than the target signal energy, no filtering is required; if the backscattered energy is much larger than the target signal energy and floods the target signal, a higher frequency modulated laser (>1 GHz) is required for high-pass filtering [19].

**Table 1.** Simulation parameters.

Parameter	Value	Unit
Total optical efficiency ( $\eta$ )	0.36	-
Receiving field of view (F)	50	mrad
Aperture (D)	0.2	m
Refractive index of seawater	1.34	-
Target distance (L)	50	m
Target reflectivity ( $\rho_t$ )	0.1	-
Attenuation coefficient ( $\alpha$ )	0.17	$\text{m}^{-1}$
Light speed in vacuum (c)	$3 \times 10^8$	m/s
Aircraft altitude (H)	1000	m
Scattering rate ( $\rho$ )	0.6	-

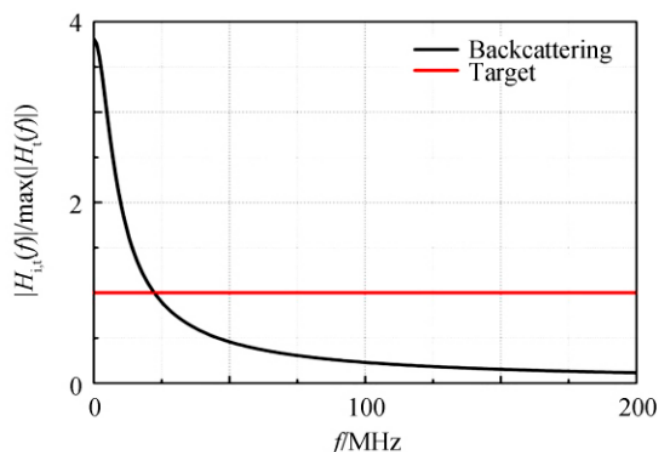


**Figure 1.** Amplitude-frequency response curve of LIDAR echo signal.

Since there is an optical transmission window of 470 nm~580 nm in seawater, in this wavelength range, 532 nm lasers are a more common type of lasers, and finally, we choose the coherent dual-frequency modulated DPS-532-B laser in the laser polarization detection system for underwater targets, and use the 532 nm wavelength of the optical band-pass filters to carry out high-efficiency filtering processing in order to achieve the purpose of suppressing underwater backscattering [20].

Two dual-frequency laser pulses with frequencies  $v_1$  and  $v_2$ , whose frequency difference is in the RF band, and the optical field can be expressed as follows:

$$E_1(v_1) = A_1 \cos(2\pi v_1 t + \phi_1) \tag{4}$$

$$E_2(v_2) = A_2 \cos(2\pi v_2 t + \phi_2) \tag{5}$$

where  $A$  and  $\phi$  are the amplitude and phase of the two light waves, and when the laser is directly incident on the photodetector, the output photocurrent is expressed as follows:

$$i(t) = [E_1(v_1) + E_2(v_2)]^2 = A_1^2 \cos^2(2\pi v_1 t + \phi_1) + A_2^2 \cos^2(2\pi v_2 t + \phi_2) + A_1 A_2 \cos[2\pi(v_1 - v_2)t + (\phi_1 - \phi_2)] + A_1 A_2 \cos[2\pi(v_1 + v_2)t + (\phi_1 + \phi_2)] \quad (6)$$

In the equation, the photodetector cannot respond to the optical frequency term and can only respond to the third RF term, generating a beat-frequency electrical signal, the shape of which is shown in Figure 2.

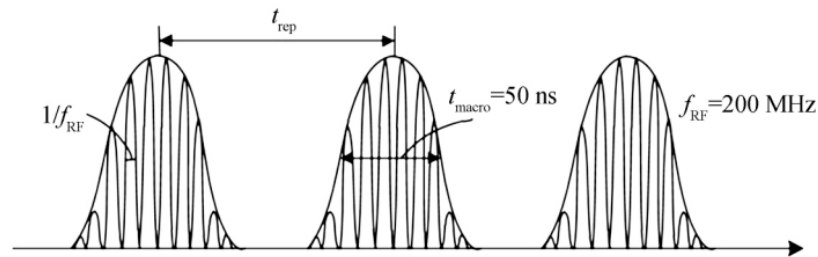


**Figure 2.** Pulse modulation time domain waveforms.

Coherent dual-frequency laser frequency difference in the radio frequency band, the frequency difference can be in the  $10^8 \sim 10^9$  Hz order of magnitude, which is equivalent to a laser pulse is high-frequency modulation, a giant pulse is modulated into many intensity fluctuations of the micro-pulse, modulation of the micro-pulse pulse width is equal to the inverse of the difference between the dual-frequency laser frequency, i.e., dual-frequency laser radio frequency difference is greater, the narrower the pulse width of the micro-pulse. This coherent dual-frequency laser can be regarded as based on the pulse internal intensity modulation technology, without the need to join the external RF modulation source, its modulation depth is deeper. Coherent dual-frequency lasers are characterized by high-frequency intensity modulation, so that most of the backscattering from seawater can be filtered out by high-pass or band-pass filtering.

The laser adopts dual-frequency injection locking, and the seed source adopts acousto-optic frequency shifting and then combining to produce dual-frequency: the light output from the narrow linewidth fiber laser is divided into two beams by the fiber coupler, and one of the beams of light passes through the acousto-optic modulator to be shifted to the central frequency of the acousto-optic modulator, setting the center frequency of the acousto-optic modulator to be  $f$ . The shifted light is combined into a beam with the light of the other beam by the other fiber coupler, and a dual-frequency laser beam containing a frequency difference of  $f$  passes through the polarizer and then is incident at a Brewster angle to the slave laser as a dual-frequency injection locked seed source. The dual-frequency laser beam with a frequency difference of  $f$  is passed through a polarizer and then incident at a Brewster angle to the slave laser as a dual-frequency injection-locked seed source [21]. The modulated pulses from the slave laser are injected into the laser amplifier for energy amplification to realize the 532 nm modulated dual-frequency pulsed green light output.

### 2.2. Measurement of Polarization Parameters

Four images with polarization directions of 0°, 45°, 90°, and 135° are taken, and their intensities are noted as I(0), I(45), I(90), and I(135), respectively, so that the line Stokes vectors of the scene can be expressed as follows [22]:

$$\begin{cases} S_0 = I(0) + I(90) \\ S_1 = I(0) - I(90) \\ S_2 = I(45) - I(135) \end{cases} \quad (7)$$

where  $S_0$  is the total light intensity of the scene, i.e.,  $I$ ,  $S_1$  is the intensity difference between the horizontal and vertical directions, and  $S_2$  is the intensity difference between the 45° and 135° directions. According to Equation (4), the expressions for the polarization degree  $p$  and polarization angle  $\theta$  can be obtained, respectively [23]:

$$p = \sqrt{S_1^2 + S_2^2} / S_0 \quad (8)$$

$$\theta = \arctan(S_2 / S_1) / 2 \quad (9)$$

## 3. System Design and Experimentation

### 3.1. Overall System Design

The polarization-based laser underwater target detection system uses the polarization information of the reflected light from the underwater target to distinguish and identify the underwater target. The laser emits laser light underwater and irradiates on the target to be measured, and its reflected light is received by the photoelectric detection equipment, which passes through the optical system therein and is received by each of the four detectors, ultimately yielding the polarization information of the object to be measured. The schematic diagram of the work that the system needs to accomplish for the measurement is shown in Figure 3. Among them, the core device of the laser underwater target polarization detection system is the photoelectric detection equipment in the dashed box. The main function of the photoelectric detection equipment is to receive the reflected light from the underwater target, correct the aberration of the light beam, split the light and change the polarization angle, and collect the polarized light information.

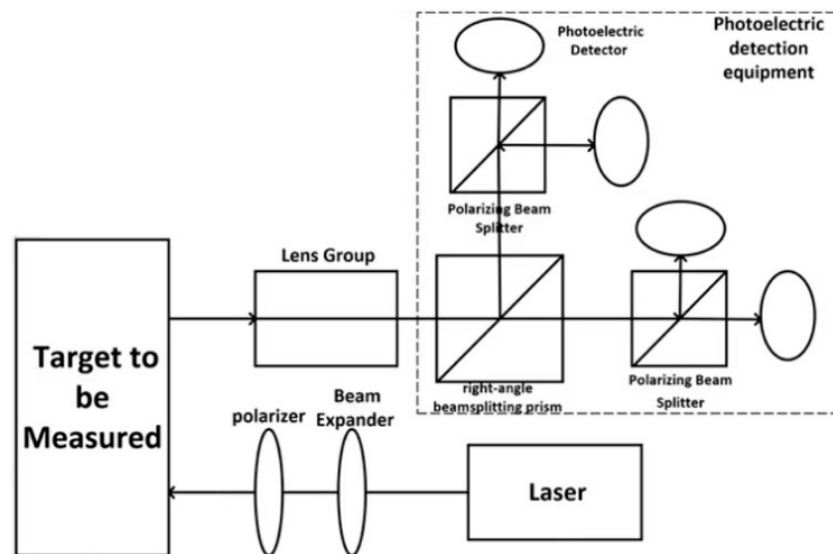


Figure 3. Schematic diagram of the working of laser polarization underwater detection equipment.

Since the natural light in the water is extremely weak, pulsed lasers are utilized for active illumination. The incident light from the laser shines on the target and is then reflected back into the photodetection equipment, through the optical system, and finally reaches the detector, completing the entire process.

### 3.2. Photodetection Design

#### 3.2.1. Optical System Design

The photoelectric detection equipment consists of two parts, the optical system and the energy detector, and the main design is shown in Figure 4: Photoelectric detection unit design. In the photoelectric detection unit, we choose a detector with a sensing area of  $10\text{ mm} \times 10\text{ mm}$ . In order to detect more accurately and reduce the spot of the laser echo, a lens set 1 is first installed in the optical system to optically converge the echo and adjust the optical path so that the laser echo can be accurately incident on the photosensitive surface of the detector. In this design, the split-amplitude method is used to measure the Stokes parameter. Firstly, the incident light is divided into two perpendicular beams by the right-angle beam-splitting prism 2. Then, the polarized light of  $0^\circ$ ,  $45^\circ$ ,  $90^\circ$ , and  $135^\circ$  is obtained by polarizing beam-splitting prisms 3 and 4, respectively, which enters into their respective energy detectors. This allows the energy values of the four detectors,  $W$ , to be substituted into Equation (7) to compute the light intensity in the four directions,  $I$ . Then, the  $I(0^\circ)$ ,  $I(45^\circ)$ ,  $I(90^\circ)$ ,  $I(135^\circ)$  are substituted into Equations (8)–(9) to calculate the polarization information of the target such as polarization degree polarization angle, respectively. At the same time, a bias detector and a 532 narrowband filter are added in front of the detector to check whether the light is polarized or not and to realize the filtering of part of the background light, so that the laser signals within a specific optical window can be received, and the interference of the noise source can be reduced, which can improve the detector's ability to extract the effective signals [24].

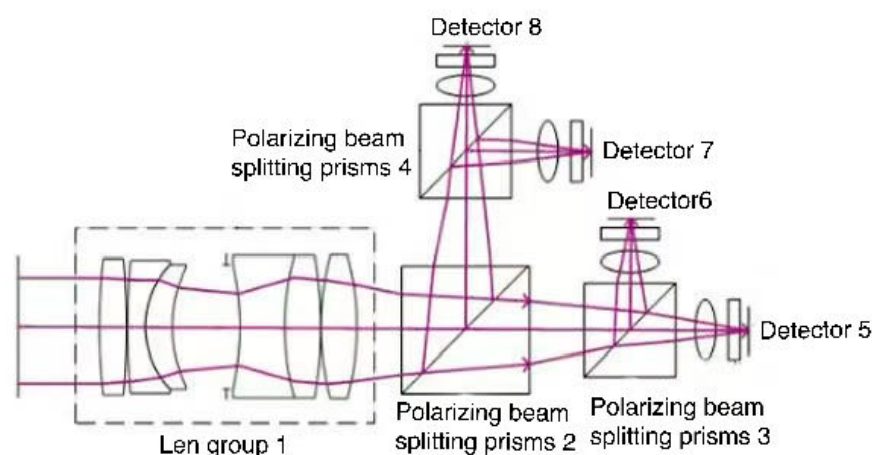


**Figure 4.** Photoelectric detection unit design.

#### 3.2.2. Optical Detection Unit Circuit Design

When designing the photodetection unit, we propose to use a PIN photodiode to receive the reflected energy of the laser because of the small energy of the detected echo and the requirement of response speed. After reviewing several photodetectors, the PIN photodiode S2387-1010R was chosen as the photodetector, and the specific characteristics of the detector are shown in Table 2 below. The PIN photodiode is an improved photoelectric device, in which the PN section of the ordinary photodiode is increased by the I-layer (filled with intrinsic semiconductors), thus increasing the wide bandwidth of the depletion layer and decreasing the effect of diffusive motion. Therefore, the PIN photodiode performance

is better than the ordinary PD tube; these performance improvements are mainly reflected in its linearity, sensitivity, reduced noise, and stable operation under low voltage, making it easier to use.

**Table 2.** Characteristic parameters of PIN detectors.

Parameter Type	Parameter Size
spectral response range	0.34~1.1 μm
rising time	3 μs
equivalent noise power	$3.1 \times 10^{-15} \text{ W/Hz}^{1/2}$
light-sensitive area	10 mm × 10 mm
conversion efficiency	0.3
light sensitivity	0.58 A/W
short-circuit current	95 μA (at 100lx)
operating temperature	-20 °C~+60 °C

From the above parameters, it can be seen that the PIN photodiode has a large sensing area, and the spectral response range includes the 532 nm laser under test. The operating principle of the PIN-type photodiode is based on the addition of a sandwich region (I-region) to the PN junction. When light is irradiated in the I-region, photogenerated carriers are generated that rapidly diffuse in the I-region to both ends and are separated and captured in the PN junction region to generate a current, thus realizing photoelectric conversion. The lower limit of energy that can be detected by this photodiode is around pJ, i.e.,  $10^{-12} \text{ J}$  order of magnitude.

The use of photoelectric detection equipment on the target’s reflected laser echo signal enables photoelectric conversion and completes the four-channel signal synchronization sampling and amplification processing. The program composition block diagram is shown in Figure 5.

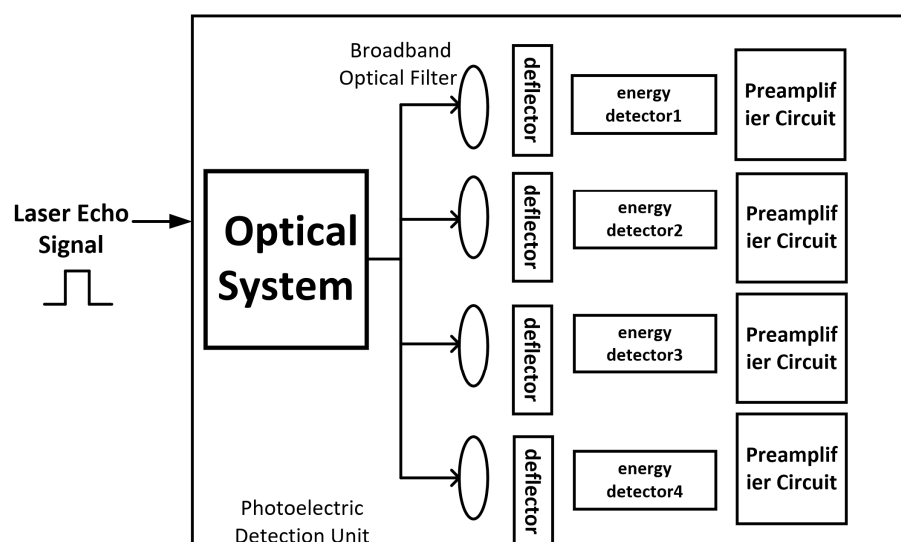


**Figure 5.** Framework diagram of program components.

### 3.3. Experimental Equipment Construction

After the structural design and machining of the detection system designed in this paper, the polarized underwater detection equipment as a whole is shown in Figure 6.



Figure 6. Framework diagram of program components.

There exists a seawater window in seawater, which has a better passage rate for blue-green band light, so the underwater polarization detection equipment selects a 532 nm laser as the light source to increase the transmitted light energy. The pool is used to build an underwater test environment, as shown in Figures 7 and 8. Different targets to be tested were placed in the pool at different distances, and the test laser passed through the 532 narrow-band filter incident into the simulated seawater environment of the pool. The laser light then traveled through the body of water and reflected off the surface of the target at  $0^\circ$ ,  $45^\circ$ ,  $90^\circ$ , and  $135^\circ$  to return with energy.

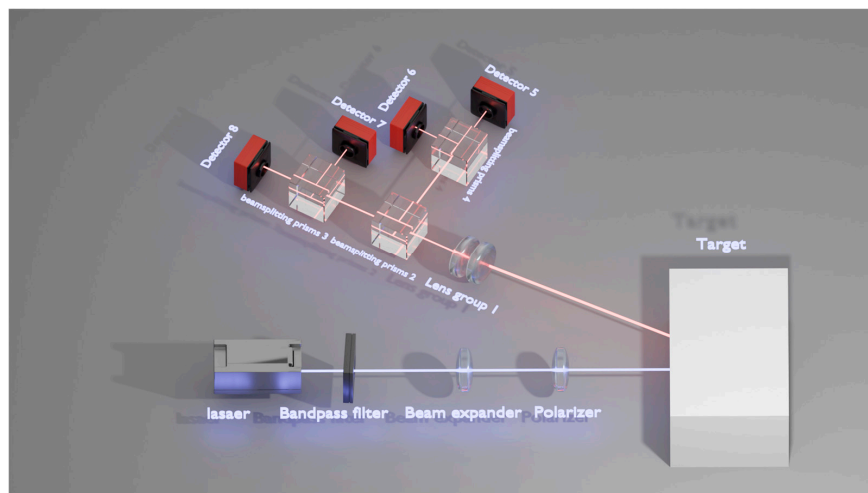


Figure 7. Underwater testing experimental setup.



Figure 8. 532 wavelength bandpass filter.

Figure 7 demonstrates the experimental setup for underwater testing designed in this study, the core of which is the photoelectric detection unit. The device consists of two parts: the optical system and the energy detector. The design concept is based on the photoelectric detection unit shown in Figure 5. The optical system contains an acousto-optic modulator (AOM) that realizes the dual-frequency modulation function, which is used for frequency separation and high-frequency modulation of the output beam of the 532 nm laser, in order to enhance the signal's immunity to interference and the target extraction efficiency.

In the optoelectronic detection unit, we chose a highly sensitive detector with a sensing area of  $10\text{ mm} \times 10\text{ mm}$ . In order to realize accurate target detection and reduce the laser echo spot, the optical system is first equipped with a lens set for beam convergence of the echo light, and the optical path is adjusted so that the laser echo can be accurately incident on the photosensitive surface of the detector. In addition, the system utilizes the fractional amplitude method to measure the Stokes parameter of the target, and its workflow is as follows:

1. The incident light is emitted by a 532 nm laser, dual-frequency modulated by an acousto-optic modulator, and then illuminated vertically onto the target surface through a band-pass filter.
2. The reflected return light from the target passes through a right-angle beam-splitting prism and is split into two mutually perpendicular beams.
3. The two beams are then passed through a polarizing beamsplitter prism and further decomposed into polarized light in the  $0^\circ$ ,  $45^\circ$ ,  $90^\circ$ , and  $135^\circ$  directions, respectively.
4. The beam in each polarization direction enters the corresponding energy detector in turn, the energy value  $W$  is recorded, and the light intensity  $I$  in each of the four directions is calculated using Equation (7).
5. Based on the light intensity values, the key information such as polarization degree and polarization angle of the target is further substituted into Equations (8) and (9).

In order to improve the signal extraction accuracy and reduce noise interference, an additional detector and a 532 nm narrowband filter are provided at the front of the detector. This design has the following advantages:

- Tests whether the incident light is polarized;
- Effectively filters out part of the background light, retaining only the laser signal within a specific optical window;
- Reduces interference from noise sources and enhances the detection efficiency of dual-frequency modulated signals.

The operation process of the whole device is as follows: after the laser is dual-frequency modulated by an acousto-optic modulator, it outputs a 532 nm laser beam, which is vertically irradiated to the target surface after passing through a band-pass filter and a beam expander. The reflected light from the target is converged and polarized by the optical system, and then received by the energy detector and analyzed for polarization, so as to obtain the polarization characteristic information of the target. By separating and analyzing the optical signals in multiple polarization directions, the system is able to accurately distinguish the material and surface characteristics of the target, while maintaining excellent anti-interference capability and detection performance under complex water conditions.

In order to simulate seawater environments at depths of 3 m, 5 m, and 10 m in the laboratory, we filled a  $10\text{ m} \times 0.5\text{ m} \times 0.5\text{ m}$  tank, as shown in Figure 9, with water. The underwater experimental environment was simulated by using the existing seawater simulation equipment in the school. The first and last ends of the tank are glass, which can pass light, and the sides of the tank are equipped with lids that can be opened so the object under test can be suspended. In this way, the laser is placed in front of the glass of the tank

to emit laser light into the tank, and the laser light can be almost vertically irradiated on the object to be measured. The underwater polarization detection equipment is placed on the back side of the target to make measurements.



**Figure 9.** 10 m × 0.5 m × 0.5 m water tanks.

Prior to conducting the experiments, calibration and performance verification of the equipment were performed to ensure the accuracy and reproducibility of the experimental setup. The calibration process included the following steps:

1. **Laser Output Calibration:** The stability of the laser output power was tested using a power meter to confirm that the laser beam maintained consistent energy at a wavelength of 532 nm.
2. **Detector Sensitivity Calibration:** The response sensitivity of the photoelectric detection unit was evaluated using a standard polarized light source to verify the detector's ability to consistently measure light signals with different polarization directions.
3. **Water Parameter Control:** The turbidity of the water was adjusted by quantitatively adding suspended particulate matter. Its stability was monitored using a turbidimeter to investigate the effects of varying turbidity levels on detection results.

During the experiment, the laser was positioned in front of the water tank's glass panel. The 532 nm laser beam was passed through a band-pass filter and beam expander before being directed vertically onto the target surface. The targets, composed of tiles, tin, and plastic, were suspended at fixed positions in the water tank at depths of 3, 5, and 10 m to ensure vertical irradiation by the laser. The laser echo signals reflected from the targets were processed by the optical system and subsequently analyzed using the polarization detection equipment. This system included Lens Set 1 for optical convergence, a polarization beam-splitting prism to separate light signals by polarization direction, and an energy detector to record the light intensity for each polarization direction.

To minimize the impact of environmental factors on the experimental results, multiple measurements were conducted for each experimental condition. Parameters such as polarization degree and polarization angle were recorded for analysis. The experiments also specifically examined the influence of the following variables on detection performance:

1. **Water Turbidity:** By varying the concentration of suspended particles in the water, the degree of interference caused by backscattering on signal detection was investigated.
2. **Target Surface Material:** The polarization characteristics of targets with varying reflectance and surface roughness were compared.

- Detection Distance: The distance between the targets and the detection equipment was adjusted to analyze the signal attenuation patterns under long-distance conditions.

Finally, the performance of the laser polarization detection device developed in this study was evaluated through multiple experimental trials. Its anti-interference capability, target recognition accuracy, and adaptability to varying detection depths in complex water conditions were thoroughly tested. These findings provide reliable data to support the practical application of the device in underwater environments.

#### 4. Experimental Results and Discussion

In order to be able to distinguish between common underwater targets, the experimental objects to be measured were selected according to different materials, including tiles, iron, and plastic, which are made of different materials and have a lot of differences in surface smoothness. Since tiles, iron sheets, and plastics belong to the objects with low transmittance and high reflectance, we place the detector end of these three samples in the direction of reflection after laser irradiation of the target, and the measurement device is shown in Figure 7.

The water used in the experiments was laboratory-standard clear water without added suspended particulate matter or other impurities, simulating a more ideal water environment. However, in real marine environments, the water usually contains different concentrations of suspended particles, dissolved particles, and impurities, and these factors can significantly affect laser propagation and polarization information extraction.

Tiles, tin, and plastic were placed at 3 m, 5 m, and 10 m for experiments, and to ensure that the experimental data were as accurate as possible, multiple sets of experiments were conducted at each depth to compare the degree of polarization of the different objects in the water, as shown in Figure 10. Then, the degree of polarization and the angle of polarization were calculated based on the energy of the four tested directions of polarization and Equations (8) and (9), and all the data were plotted in Table 3.

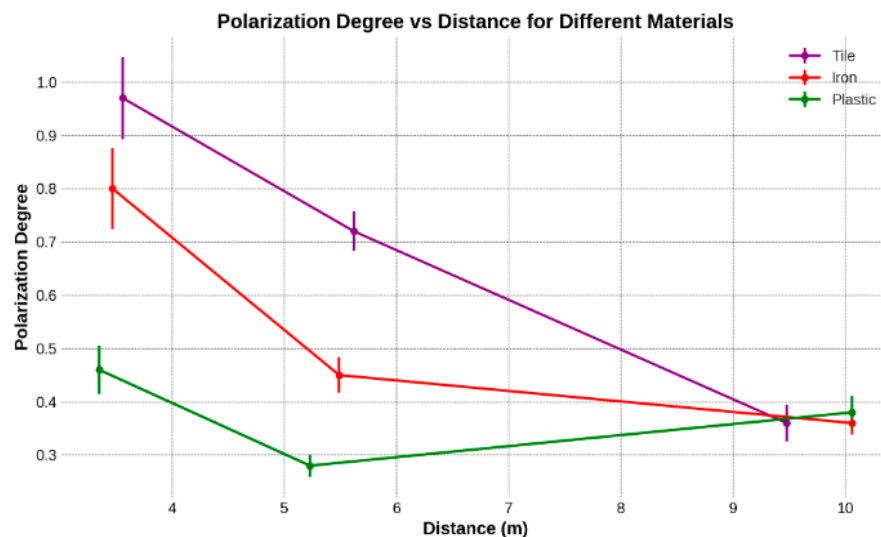


Figure 10. Compare the degree of polarization of different objects in water.

**Table 3.** Underwater polarization measurement data.

Distance (m)	0° (J)	45° (J)	90° (J)	135° (J)	Polarization	Angle of Polarization
tiles						
3	$6.85 \times 10^{-11}$	$3.19 \times 10^{-11}$	$8.2 \times 10^{-11}$	$2.2368 \times 10^{-10}$	0.95	42.99
5	$9.27 \times 10^{-10}$	$7.67 \times 10^{-12}$	$1.39 \times 10^{-9}$	$1.3069 \times 10^{-9}$	0.76	35.10
10	$9.63 \times 10^{-10}$	$5.41 \times 10^{-10}$	$1.1 \times 10^{-9}$	$1.2187 \times 10^{-9}$	0.36	39.30
galvanized iron sheets (for building construction)						
3	$6.99 \times 10^{-11}$	$3.25 \times 10^{-11}$	$1.99 \times 10^{-10}$	$2.279 \times 10^{-10}$	0.88	28.32
5	$1.9 \times 10^{-10}$	$2.35 \times 10^{-10}$	$3.37 \times 10^{-10}$	$3.71 \times 10^{-10}$	0.46	21.45
10	$1.97 \times 10^{-10}$	$2.04 \times 10^{-10}$	$3 \times 10^{-10}$	$3.64 \times 10^{-10}$	0.35	28.66
plastics						
3	$7.71 \times 10^{-10}$	$4.82 \times 10^{-10}$	$8.35 \times 10^{-10}$	$1.27 \times 10^{-9}$	0.47	42.69
5	$7.02 \times 10^{-10}$	$6.4 \times 10^{-10}$	$9.23 \times 10^{-10}$	$1.06 \times 10^{-9}$	0.28	31.02
10	$7.85 \times 10^{-10}$	$4.89 \times 10^{-10}$	$7.81 \times 10^{-10}$	$1.09 \times 10^{-9}$	0.38	44.80

As can be seen from Table 3, in the underwater test target polarization, plastic polarization is the lowest, followed by tin, and the highest polarization is tile. Test results at 3 m show that the polarization of different materials varies greatly; with the increase in distance, their polarization degrees finally approach 0.36 or so. This phenomenon may be due to the experiments used in the pool being relatively narrow and long; with the increase in distance, the laser underwent multiple reflections and scattering by the water body and the pool wall, resulting in the final receding polarization effect being relatively close to each other. When the distance is closer, the main factor causing the change in polarization degree is dominated by the polarization characteristics of the target reflection, so the polarization degree of the reflected light varies more when the distance is closer.

In order to further verify the reliability of the measurement method of this detection device, the test environment was emptied of water, and the polarization was measured repeatedly in the air medium on the target under test. The target was placed at a distance of 10 m from the laser for the test due to the negligible loss of laser propagation in the air, and the results of the measured and calculated polarization are shown in Table 4.

**Table 4.** Airborne polarization measurements.

Distance (m)	0° (J)	45° (J)	90° (J)	135° (J)	Polarization	Angle of Polarization
tiles						
10.033	$7.06 \times 10^{-11}$	$3.29 \times 10^{-11}$	$1.99 \times 10^{-10}$	$2.47 \times 10^{-10}$	0.91	29.52
galvanized iron sheets (for building construction)						
10.029	$1.79 \times 10^{-9}$	$9.49 \times 10^{-10}$	$2.43 \times 10^{-9}$	$3.27 \times 10^{-9}$	0.57	37.32
plastics						
10.033	$2.48 \times 10^{-10}$	$2.42 \times 10^{-10}$	$3.76 \times 10^{-10}$	$5.65 \times 10^{-10}$	0.49	34.16

From Table 4, it can be seen that the order of the polarization size of the target in the air is consistent with the underwater test results, and the polarization of the same target in different media does not differ much. Analyzing the reasons, the surface of plastic is rougher, the reflectivity is lower, resulting in lower polarization; iron, as a metal material, has smaller retreat polarization and smoother surface, so the polarization is higher; tiles are characterized by their irregular molecular structure, which will randomly change the vibration direction of the light when it passes through, resulting in the transmission of polarized light in multiple directions, forming a higher overall polarization.

To further evaluate the stability of the experimental results and the reliability of the measurements, we calculated the 95% confidence intervals for the polarization values and analyzed the fluctuation ranges of polarization for different materials under varying distance conditions. The results indicate that the 95% confidence interval for the polarization of tiles at 3 m (0.95) is [0.92, 0.98], while the confidence interval for the polarization of plastics at 10 m (0.38) is [0.30, 0.46]. The analysis of these confidence intervals highlights significant differences in the effect of water depth on the polarization characteristics of different materials, particularly at longer distances (e.g., 10 m), where the polarization differences between materials become less pronounced.

In order to quantify the effect of distance on polarizability, we performed a regression analysis between polarizability and distance. By building a linear regression model, the results showed a significant negative correlation between polarizability and distance ( $R^2 = 0.87$ ), as specified in the following equation:

$$\text{Polarization} = 0.92 - 0.05 \times \text{distance (m)}$$

This model shows that the polarization gradually decays with increasing distance, whereas tiles and tin maintain high polarization at short distance conditions, while the polarization of plastic changes more significantly. This regression model provides an important quantitative basis for assessing the attenuation of polarized signals underwater.

To further validate the performance of the laser polarization detection equipment designed in this study, we compared the experimental results with relevant findings in the literature. Mou Chang et al. [20] in their 2018 study systematically demonstrated the polarization characteristic differences among underwater targets with varying materials and surface structures by constructing a detection system based on polarization information. Their experiment employed a 532 nm wavelength laser as an active emission source, combined with polarization detection techniques, to analyze the polarization characteristics of reflected light. The results showed that the polarization degree of reflected light from man-made targets was significantly higher than that of natural targets (e.g., aquatic plants), thereby proving the feasibility of underwater target detection using polarization information.

In comparison, this study achieved a polarization degree of 0.95 for ceramic tiles at a detection distance of 3 m, surpassing the maximum polarization degree of approximately 0.85 reported by Mou et al. This difference likely stems from significant advancements in this study, particularly the use of dual-frequency modulated 532 nm lasers for suppressing backscattering and effectively extracting polarization information. Furthermore, this study extended the detection range, demonstrating that the equipment could still differentiate between different target materials at a distance of 10 m, whereas Mou et al.'s research primarily focused on shorter distances. This advantage may be attributed to the optimized optical system design in this study, including the application of efficient narrow-band filters and advanced dual-frequency modulation signal processing techniques, enabling stronger anti-interference capabilities and clearer polarization data capture.

Additionally, this study verified the stability and consistency of the equipment across different media, such as water and air. Experimental results indicate that the order of polarization degrees among targets remains consistent in both media, confirming the reliability of the equipment under varying conditions. Specifically, plastic exhibited the lowest polarization degree due to its rough surface and low reflectivity, while metal sheets, such as iron, had higher polarization degrees due to their smooth surfaces and minimal depolarization effects. Ceramic tiles demonstrated the highest polarization degree, attributed to their amorphous molecular structure, which randomly alters the vibration direction of

light, resulting in polarized light transmission in multiple directions and an overall high polarization degree.

Compared to traditional laser detection techniques, the laser polarization detection equipment developed in this study significantly enhances underwater target identification accuracy and detection depth. Its superior performance in complex environments exceeds the results reported in existing literature. This technical advantage not only provides robust support for future underwater target detection but also lays the foundation for achieving more efficient and cost-effective underwater detection solutions.

In summary, the equipment developed in this study demonstrates substantial improvements in suppressing backscattering, enhancing the polarization information of reflected light, and extending the detection range. These advancements complement and elevate the findings of Mou et al.'s work. The reliability of the laser polarization detection equipment in complex underwater environments has been thoroughly validated, offering valuable experimental and theoretical support for further optimization and broader adoption of polarization-based underwater detection technologies.

## 5. Conclusions

In this study, a laser polarization underwater detection device is designed and experimentally verified. The basic principle of underwater laser detection and the implementation method of polarization measurement are introduced, and a dual-frequency modulated 532 nm laser is used to effectively suppress the backward scattering in the underwater environment by using the polarization characteristics of the pulsed laser, which significantly improves the accuracy and depth of target detection. The experimental results show that the system can easily distinguish targets of different materials, and verify the consistent results of target detection under different media. In addition, the present technique demonstrates excellent adaptability in a real water environment, which is of great significance for the development and safety of the ocean and rivers. In the future, this study aims to further explore the integration of laser polarization detection technology with other underwater imaging systems to achieve more efficient and lower-cost underwater detection solutions, providing strong technical support for global ocean mapping and underwater engineering monitoring.

**Author Contributions:** Conceptualization, Q.H.; Methodology, C.D.; Formal analysis, J.D.; Investigation, X.G., J.L., G.D. and H.Z.; Resources, L.Z.; Writing—original draft, F.Z.; Writing—review & editing, Q.F.; Supervision, Y.Z. All authors have read and agreed to the published version of the manuscript.

**Funding:** Based on combining of laser-induced acoustics effect and blue-green laser communication for establishing the two-way new communications system access the boundary of air-sea (Nos U22A2008), and National Natural Fund Joint Fund Program (Nos U2341226).

**Institutional Review Board Statement:** Not applicable.

**Informed Consent Statement:** Not applicable.

**Data Availability Statement:** The data supporting the findings of this study are not publicly available due to privacy. However, they are available from the corresponding author upon reasonable request.

**Acknowledgments:** First and foremost, I would like to express my sincere gratitude to my supervisor, Qiang Fu, for his invaluable support and guidance throughout the course of this research. His meticulous guidance, insightful advice, and constant encouragement have greatly influenced my progress in the field of research. I am also deeply grateful to Li Zheng for providing me with crucial resources and guidance on the research direction. His valuable insights helped me to clarify the focus of my study and gave me a deeper understanding of the subject. My sincere thanks go to

Dong Geng, Xiansong Gu, Jianhua Liu, and Haili Zhao, whose contributions in the investigation phase were essential to the success of this study. Their collaborative efforts allowed us to overcome many technical challenges, ensuring the smooth progress of the research. I would like to express my appreciation to Chao Dong for his critical support in methodology design. His help in constructing the research framework and experimental protocols played a key role in the success of this project. I also thank Jin Duan for his excellent work in data analysis. His skills were instrumental in unlocking the potential of the research data and revealing key findings. Finally, I would like to thank Yong Zhu for his continuous guidance and supervision throughout this study, ensuring that the research remained on track and leading to its successful completion.

**Conflicts of Interest:** The authors declare no conflict of interest.

## References

1. Yang, H.; Liang, Y. Current status and prospect of airborne blue-green laser underwater target detection technology. *Opt. Mech. Inf.* **2003**, *12*, 6–10.
2. Song, Y.; Liang, J. A review of airborne laser bathymetry data processing research. *Surv. Mapp. Spat. Geogr. Inf.* **2023**, *46*, 45–47+53.
3. Wang, W.; Feng, W.; Zhu, Z.; Liu, Y.; Chen, H.; Zhang, Q.; Huang, X.; Zhao, L.; Yang, T.; Guo, J.; et al. Research on underwater imaging technology of sea ranch based on laser polarization technology. *Optoelectron.-Laser* **2021**, *32*, 581–586. [[CrossRef](#)]
4. Zong, S.; Yang, S.; Liang, S. Method for Detecting Underwater Microbubbles Using Dual-Mode Fusion of Laser Polarization. *Appl. Sci.* **2024**, *14*, 8465. [[CrossRef](#)]
5. Lewis, G.D.; Jordan, D.L.; Roberts, P.J. Backscattering target detection in a turbid medium by polarization discrimination. *Appl. Opt.* **1999**, *38*, 3937–3944. [[CrossRef](#)] [[PubMed](#)]
6. Kushina, M.E.; Heberle, G.; Hope, M.; Hall, D.; Bethel, M.; Calmes, L.K. ALMDS Laser System. In Proceedings of the SPIE 4968, Solid State Lasers XII, High-Power Lasers and Applications, San Jose, CA, USA, 25–31 January 2003; pp. 163–168. [[CrossRef](#)]
7. Brian, B.; Abbot, R.H.; Penny, M.F. Airborne estimation of sea turbidity parameters from the WRELADS laser airborne depth sounder. *Appl. Opt.* **1986**, *25*, 2080.
8. Setter, C.; Willis, R.J. LADS—From Development to Hydrographic Operation. In Proceedings of the U.S. Hydrographic Conference, San Diego, CA, USA, 18 April 1994; pp. 134–143.
9. Ouyang, B.; Dalgleish, F.R.; Caimi, F.M.; Giddings, T.E.; Shirron, J.J.; Vuorenkoski, A.K.; Nootz, G.; Britton, W.; Ramos, B. Underwater laser serial imaging using compressive sensing and digital mirror device. *Proc. SPIE* **2011**, *8037*, 168–241.
10. Schechner, Y.Y.; Karpel, N. Recovery of underwater visibility and structure by polarization analysis. *IEEE J. Ocean. Eng.* **2005**, *30*, 570–587. [[CrossRef](#)]
11. Schechner, Y.Y.; Karpel, N. Clear underwater vision. In Proceedings of the 2004 IEEE Computer Society Conference on Computer Vision and Pattern Recognition, Washington, DC, USA, 27 June–2 July 2004; pp. 167–196.
12. Namer, E.; Schechner, Y.Y. Advanced visibility improvement based on polarization filtered images. *Proc. SPIE* **2005**, *5888*, 36–45.
13. Hufnagel, F.; Sussman, B.J. Characterization of an underwater channel for quantum communications in the Ottawa River. *Opt. Express* **2019**, *27*, 26346. [[CrossRef](#)] [[PubMed](#)]
14. Cherian, A.K.; Poovammal, E. A Novel AlphaSRGAN for Underwater Image Super Resolution. *Comput. Mater. Contin.* **2021**, *69*, 1537–1552. [[CrossRef](#)]
15. Cochenour, B.; Mullen, L.; Muth, J. Modulated pulse laser with pseudorandom coding capabilities for underwater ranging, detection, and imaging. *Appl. Opt.* **2011**, *50*, 6168–6178. [[CrossRef](#)] [[PubMed](#)]
16. Stokes, G.G. On the Change of Refrangibility of Light. *Philos. Trans. R. Soc. Lond.* **1852**, *142*, 463–562. [[CrossRef](#)]
17. Sulimov, B.V. Absorption of light by a ferromagnetic semiconductor. *Sov. Phys. J.* **1975**, *17*, 662–666. [[CrossRef](#)]
18. Smith, J.; Johnson, L. *Advanced Engineering Mathematics*, 3rd ed.; Oxford University Press: Oxford, UK, 2008; pp. 154–196.
19. Song, T.; Zhang, B.; Luo, Q. Design and Optimization of Optoelectronic Conversion Circuits. *Appl. Optoelectron. Technol.* **2010**, *25*, 46–48.
20. Chu, N.; Cao, L.; Huang, W. Response time analysis of PIN photodiodes based on light intensity. *J. Sens. Technol.* **2013**, *26*, 34–37.
21. Qian, C.; Min, Y.W.; Luo, Y.Z. Analysis of the polarization characteristics of scattered light of underwater suspended particles based on Mie theory. *Optoelectron. Lett.* **2021**, *17*, 252–256.
22. Mou, C.; Wang, C.; Duan, K.; Zhang, L.; Li, Y.; Chen, H.; Liu, J.; Zhao, Q.; Sun, M.; Yang, X.; et al. Research on laser underwater target detection technology based on polarization information. *J. Chang. Univ. Sci. Technol.* **2018**, *41*, 86–89.
23. Bao, F.; Duan, J.; Dong, S.; Ma, L.; Yu, T.; Zhan, J. Experimental study on polarization imaging characteristics of underwater targets. *J. Appl. Opt.* **2019**, *40*, 27–32. [[CrossRef](#)]
24. Liang, X. Experimental Study on Polarization Imaging of Streak Tube Lidar. Ph.D. Thesis, Harbin Institute of Technology, Harbin, China, 2010.

---

**Disclaimer/Publisher's Note:** The statements, opinions and data contained in all publications are solely those of the individual author(s) and contributor(s) and not of MDPI and/or the editor(s). MDPI and/or the editor(s) disclaim responsibility for any injury to people or property resulting from any ideas, methods, instructions or products referred to in the content.